

The Low-lying Dirac Eigenmodes from Domain Wall Fermions

Guofeng Liu^{a*} [RBC colabration]

^aDepartment of Physics, Columbia University, New York, NY, 10027, USA

We calculate the low-lying eigenvalues and eigenvectors of the hermitian domain wall Dirac operator on various gauge backgrounds by Ritz minimization. The mass dependence of these eigenvalues is studied to extract the physical 4 dimensional λ , whose spectral density is related to $\langle\bar{\psi}\psi\rangle$ through the Banks-Casher relation, and δm , which represents the effects of the residual chiral symmetry breaking in domain wall formalism on a per eigenmode basis. The topological structure of the underlying gauge field is examined by measuring the Γ_5 matrix elements between the low-lying eigenmodes.

1. DIAGONALIZATION METHOD

We use the conjugate-gradient method proposed by Kaukreuter and Simma [1]² to calculate the lowest 19 eigenvalues and eigenvectors of the hermitian domain wall Dirac operator $D_H = \gamma_5 R D$, where D is the domain wall Dirac operator and R is the reflection operator in s direction (look at [2] for a detailed description of the conventions).

Table 1

The bare quark masses used for the Wilson ensembles are 0.0, 0.0025, 0.005, 0.0075, 0.01. For the Iwasaki ensemble, only the lowest mass, 0.0005, is different.

V	Action	β	a^{-1}/Gev	L_s	#conf.
16 ⁴	Wilson	6.0	2.0	16	32
16 ⁴	Wilson	6.0	2.0	8	10
16 ⁴	Iwasaki	2.6	2.0	16	55

For each of the configurations listed in Table 1., we calculate the eigenvalue spectrum at five different masses. There are two main reasons for this practice. First, by studying the mass dependence as described in section 2, we can remove from the eigenvalue spectrum a portion of the residual chiral symmetry breaking effects. For the Iwasaki action at $\beta = 2.6$, the residual mass is very small, which makes the convergence of the Ritz minimization prohibitively slow at zero bare

quark mass. Thus, we had to use nonzero bare quark masses (5×10^{-4} and up) to speed up the convergence, and then extrapolate to the region of interest.

2. SPECTRAL DENSITY AND CHIRAL SYMMETRY BREAKING

In the continuum limit, the spectral density of Dirac operator is related to the chiral condensate $\langle\bar{\psi}\psi\rangle$ by the Banks-Casher relation

$$-\langle\bar{\psi}\psi\rangle = \frac{1}{12V} \frac{\langle|\nu|\rangle}{m} + \frac{1}{12V} \left\langle \sum_{\lambda \neq 0} \frac{m}{\lambda^2 + m^2} \right\rangle \quad (1)$$

and

$$\lim_{m \rightarrow 0} \lim_{V \rightarrow \infty} -\langle\bar{\psi}\psi\rangle = \frac{\pi}{12} \rho(0). \quad (2)$$

Since D_H is a continuous function of m_f , we can expand and parameterize its eigenvalue $\Lambda_{H,i}$ as

$$\Lambda_{H,i}^2 = n_{5,i}^2 (\lambda_i^2 + (m_f + \delta m_i)^2) + O(m_f^3). \quad (3)$$

From

$$\frac{dD_H}{dm_f} = -\gamma_5 Q^{(w)}, \quad (4)$$

where $-m_f R Q^{(w)}$ is the mass term in the fermion matrix, we can derive

$$-\langle \Lambda_{H,i} | \gamma_5 Q^{(w)} | \Lambda_{H,i} \rangle = \frac{d\Lambda_{H,i}}{dm_f} \quad (5)$$

$$= \frac{n_{5,i}^2 (m_f + \delta m_i)}{\Lambda_{H,i}} \quad (6)$$

*This work was supported in part by the Department of Energy and the RIKEN BNL Research Center.

²QCDSP implementation by Robert Edwards.

The quantity $\langle \bar{\psi}\psi \rangle$ is defined on the boundary for domain wall fermions, and given by

$$-\langle \bar{q}q \rangle = -\frac{1}{12V} \left\langle \sum_{\Lambda_H} \frac{\langle \Lambda_H | \gamma_5 Q^{(w)} | \Lambda_H \rangle}{\Lambda_H} \right\rangle \quad (7)$$

$$= \frac{1}{12V} \left\langle \sum_i \frac{m_f + \delta m_i}{\lambda_i^2 + (m_f + \delta m_i)^2} \right\rangle. \quad (8)$$

By comparing Eq. 8 and Eq. 1, we can recognize the parameter λ_i as an eigenvalue of the four dimensional Dirac operator. Here, δm_i represents the contribution to the eigenvalue from the chiral symmetry breaking effects of coupling of the domain walls.

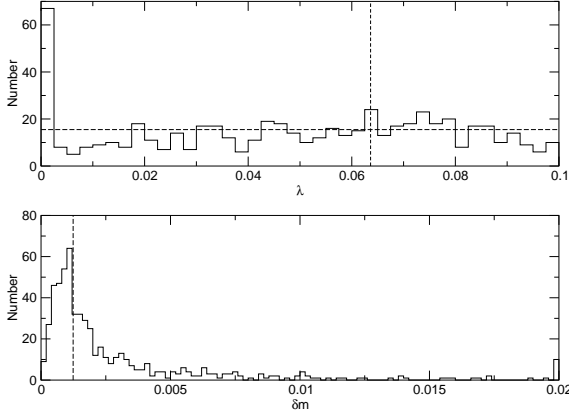


Figure 1. λ and δm distribution for the Wilson ensemble at $\beta = 6.0$, $L_s = 16$. The horizontal line in the upper panel is $\rho(0)$ calculated from $\langle \bar{\psi}\psi \rangle$ using Eq. 2. The vertical line in the upper panel is the minimum of the largest λ in each configuration, which means there is no error introduced by dropping higher modes to the left of this line. The vertical line in the lower panel is the residual mass determined independently from the midpoint Ward/Takahashi identity term.

Fig. 1, 2 and 3 are the distribution of λ and δm for the ensembles listed in Table 1. A rough agreement between the peak of the δm distribution and m_{res} from the mid-point term is observed. A nice agreement between the spectral density and $\langle \bar{\psi}\psi \rangle$ is confirmed except for the peak at $\lambda = 0$, which is explained by the abundance of zero modes at

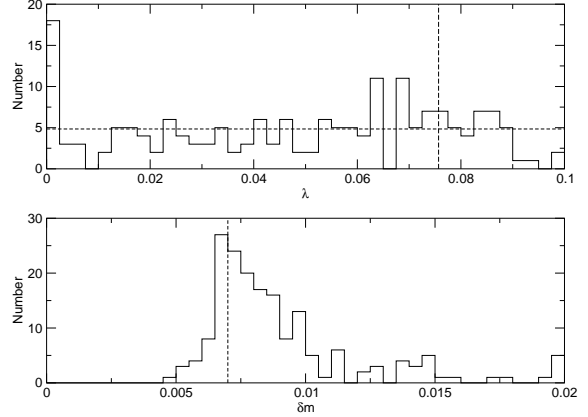


Figure 2. λ and δm distribution for Wilson ensemble at $\beta = 6.0$, $L_s = 8$.

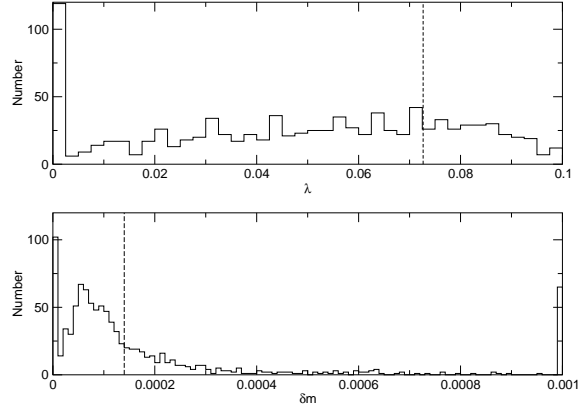


Figure 3. λ and δm distribution for Iwasaki ensemble at $\beta = 2.6$, $L_s = 16$.

finite volume, and is expected to disappear in the infinite volume limit. The comparison between Fig 1 and 2 shows the expected L_s dependence of δm . Fig 1 and 3 have the same L_s , volume and strength of coupling but different types of action, which makes the δm an order of magnitude smaller for the latter.

3. GAUGE FIELD TOPOLOGICAL STRUCTURE

In the continuum limit, the Dirac operator has γ_5 symmetry, which ensures that the zero modes have chirality of ± 1 , and the non-zero modes, with chirality 0, are paired by the application of γ_5 . The number of zero modes should correspond

to the winding number of the gauge field.

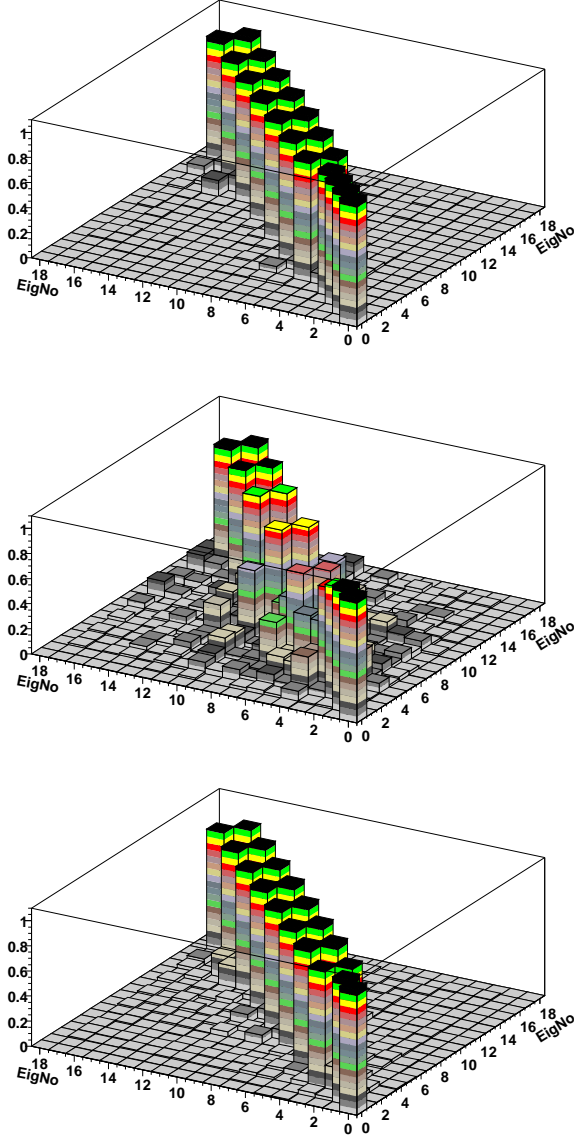


Figure 4. Lego plots of three sequential configurations separated by 3 and 4 heat bath sweeps.

In the domain wall formalism, we display the matrix elements $|\langle \Lambda_{H,i} | \Gamma_5 | \Lambda_{H,j} \rangle|$ as a 3 dimensional lego plot. This provides a way of visualizing the chiral properties of the domain wall Dirac operator and the topological structure of the underlying gauge field. Fig 4 shows a set of such lego plots for the Wilson ensemble at $\beta = 6.0$,

$L_s = 16$. In the first lego plot, the lowest 4 of the eigenvectors are also Γ_5 eigenvectors, while the rest of them are paired. Fig 4 also shows that during the heat bath evolution, when a configuration transforms from the topological sector with topology 4 to that with topology 2, some complex configurations result in between which can not be unambiguously categorized as belonging to any regular topological sector. Table 2 lists the percentage of this kind of complex configuration for each ensemble in Table 1. The readers are referred to C. Dawson's poster for a more quantitative study of the complex configurations.

Table 2

List of the values of m_{res} and percentage of complex configurations.

Action	β	L_s	m_{res}	complex%
Wilson	6.0	16	0.00124(5)	50%
Wilson	6.0	8	~ 0.007	50%
Iwasaki	2.6	16	0.00014(3)	10%

4. CONCLUSIONS

Our prescription of extracting λ and δm distribution from mass dependence of the eigenvalues of D_H is consistent with the Banks-Casher relation and the usual ways of determining $\langle \bar{\psi}\psi \rangle$ and m_{res} . The good chiral properties of domain wall fermions makes them a very good tool for studying the topological structure of the background gauge field. We find that this structure is closely related to the type of action used in generating these configurations.

5. ACKNOWLEDGMENT

These calculations were performed on the QCDSP machines at Columbia and the RIKEN BNL Research Center.

REFERENCES

1. T. Kalkreuter and H. Simma, hep-lat/9507023
2. T. Blum *et. al.*, hep-lat/0007038.